Parity violation in proton-proton scattering at 221 MeV

A. R. Berdoz,[1] J. Birchall,[1] J. B. Bland,[1] J. D. Bowman,[2] J. R. Campbell,[1] G. H. Coombes,[3] C. A. Davis,[1,3] A. A. Green,[1] P. W. Green,[4] A. A. Hamian,[1] R. Helmer,[3] S. Kadantsev,[3] Y. Kuznetsov,[5,*] L. Lee,[1] C. D. P. Levy,[3] R. E. Mischke,[2] N. T. Okumusoglu,[6] S. A. Page,[1] W. D. Ramsay,[1] S. D. Reitzner,[1] T. Ries,[3] G. Roy,[4] A. M. Sekulovich,[1] J. Soukup,[4] G. M. Stinson,[4] T. J. Stocki,[4] V. Sum,[1] N. A. Titov,[5] W. T. H. van Oers,[1] R. J. Woo,[1] S. Zadorozny,[5] and A. N. Zelenski[5]

(TRIUMF E497 Collaboration)

[1]*Department of Physics and Astronomy, University of Manitoba, Winnipeg, Manitoba, Canada R3T 2N2*

[2]*Physics Division, Los Alamos National Laboratory, Los Alamos, New Mexico 87545, USA*

[3]*TRIUMF, 4004 Wesbrook Mall, Vancouver, British Coulmbia, Canada V6T 2A3*

[4]*Centre for Subatomic Research, University of Alberta, Edmonton, Alberta, Canada T6G 2N5*

[5]*Institute for Nuclear Research, Academy of Sciences of Russia, RU-117334 Moscow, Russia*

[6]*Rize Faculty of Sciences and Arts, Karadeniz Technical University, Rize, Turkey*

(Received 20 November 2002; revised manuscript received 30 May 2003; published 23 September 2003)

TRIUMF experiment 497 has measured the parity-violating longitudinal analyzing power A_z in $\vec{p}p$ elastic scattering at 221.3 MeV incident proton energy. This comprehensive paper includes details of the corrections, some of magnitude comparable to A_z itself, required to arrive at the final result. The largest correction was for the effects of first moments of transverse polarization. The addition of the result, $A_z=[0.84\pm0.29\ (\text{stat.})\pm0.17\ (\text{syst.})]\times10^{-7}$, to the $\vec{p}p$ parity-violation experimental data base greatly improves the experimental constraints on the weak meson-nucleon coupling constants h_ρ^{pp} and h_ω^{pp}, and also has implications for the interpretation of electron parity-violation experiments.

DOI: 10.1103/PhysRevC.68.034004 PACS number(s): 21.30.Cb, 11.30.Er, 24.70.+s, 25.40.Cm

I. INTRODUCTION

This experiment determines the parity-violating longitudinal analyzing power, $A_z=(\sigma^+-\sigma^-)/(\sigma^++\sigma^-)$, in $\vec{p}p$ elastic scattering, where σ^+ and σ^- are the scattering cross sections for positive and negative helicity. The measurements were performed in transmission geometry, with beam energy and detector geometries selected to ensure that parity mixing in the lowest order $^1S_0$-$^3P_0$ partial wave amplitude did not contribute to the measured A_z, hence leaving a parity-violating asymmetry arising almost entirely from $^3P_2$-$^1D_2$ mixing [1]. This amplitude has not previously been studied experimentally, and the possibility is unique to the energy regime accessible with the TRIUMF cyclotron. The energy at which the contribution to A_z from the lowest order $^1S_0$-$^3P_0$ mixing vanishes is determined by the well known strong nuclear phase shifts. The scale factors multiplying this and other partial wave contributions are set by the weak interaction. $\vec{p}p$ parity-violation experiments determine these scale factors experimentally. In the context of the weak meson exchange model [2], the TRIUMF measurement of A_z determines primarily the weak ρ-meson-nucleon coupling constant $h_\rho^{pp}=(h_\rho^0+h_\rho^1+h_\rho^2/\sqrt{6})$, where the superscripts refer to isospin change [3]. Precision results already obtained by the SIN group at 45 MeV [4] and the Bonn group at 13.6 MeV [5] determined essentially the sum $h_\rho^{pp}+h_\omega^{pp}$, where $h_\omega^{pp}=h_\omega^0+h_\omega^1$. With the addition of the TRIUMF result at 221.3 MeV, h_ρ^{pp} and h_ω^{pp} are now determined separately for the first time.

It is important to have experimentally determined values of the weak meson-nucleon couplings, as theoretical calculations of their values are quite uncertain and the correct values are helpful in the interpretation of the results of other parity-violation experiments. They are needed, for example, in calculations of the proton anapole moment [6], one of the radiative corrections to the electron-nucleon isovector axial form factor in experiments such as SAMPLE [7] and G^0 [8].

II. BACKGROUND

TRIUMF E497 [9], was first funded in 1988, and the required new beam line was completed in 1994. A major effort to understand and minimize systematic error contributions was then undertaken. Following many years of effort that resulted in the reduction of both the helicity-correlated beam modulations Δx_i and the sensitivities $\partial A_z/\partial x_i$ to these modulations, the first significant dataset for E497 was acquired in February and March of 1997, with a statistical error on A_z of $\pm0.5\times10^{-7}$, and most systematic errors at or below the 10^{-7} level. That result represented a major milestone for the experiment [10]. Data taking continued in 1998 and 1999, the final reanalysis of all the data was completed in early 2001 [11], and the result for A_z was published [12]. The present paper presents detailed descriptions of the experiment, the data analysis and systematic error corrections, that were not included in the paper [12].

III. EXPERIMENTAL SETUP

A. General

The principle of the experiment is straightforward. A longitudinally polarized proton beam is passed through a liquid

*Deceased.

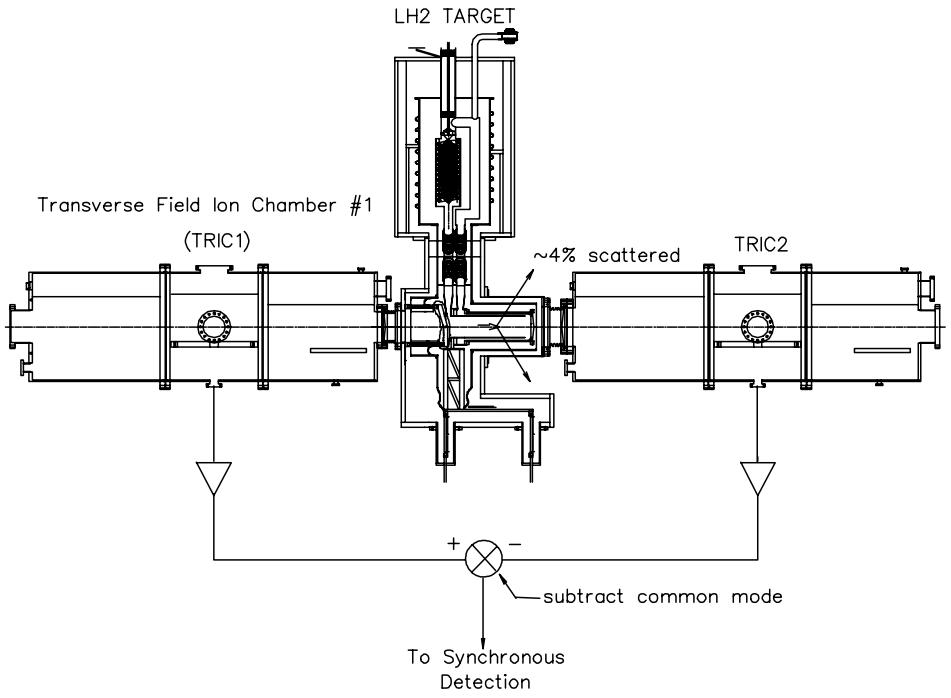

FIG. 1. Principle of the measurement. A longitudinally polarized proton beam was passed through a liquid hydrogen target. The beam current before and after target was detected and the signals were subtracted. The presence of a component of the difference signal synchronized with spin flip indicates a parity-violating dependence of the transmission through the target on the helicity of the incident protons.

hydrogen target and the change in transmission when the spin of the incident protons is reversed is the parity-violating signal. To measure this, the beam current before and after the liquid hydrogen target was measured and the signals were subtracted (Fig. 1). The spin state was then changed in a special pattern at 40 spin states per second and synchronous detection was used to extract that component of the difference signal that was synchronized with the spin flip. Unfortunately, beam parameters other than spin changed when the spin was flipped, and great pains had to be taken to measure and correct for the false signals resulting from these unwanted helicity-correlated changes. Technical details of the systems required to do this will be described in detail in what follows, but an idea of the complexity can be obtained from Fig. 2, identifying the major pieces of equipment, and Fig. 3, showing the sequencing of the control measurements within a 200 ms, eight spin-state cycle.

Because of the importance of understanding systematic errors in such an experiment, essentially all the pieces of equipment, from the ion source to the beam dump, had to be considered integral parts of the parity experiment. Figure 2 shows the main subsystems of the experiment—the TRIUMF optically pumped polarized ion source (OPPIS), the cyclotron, the beam transport, and the specialized parity instrumentation [13]. A 5 μA transversely polarized beam was transported to the cyclotron through an $\approx$50-m-long injection beam line. A 200-nA beam at 75%–80% vertical polarization was extracted at 221.3 MeV. Spin precession through pairs of solenoid and dipole magnets resulted in delivery of a longitudinally polarized beam to the parity apparatus. There were two complementary states of the spin transport, the ''positive helicity'' and ''negative helicity'' beam line tunes, which transported spin up in the cyclotron into either + or − helicity at the parity apparatus.

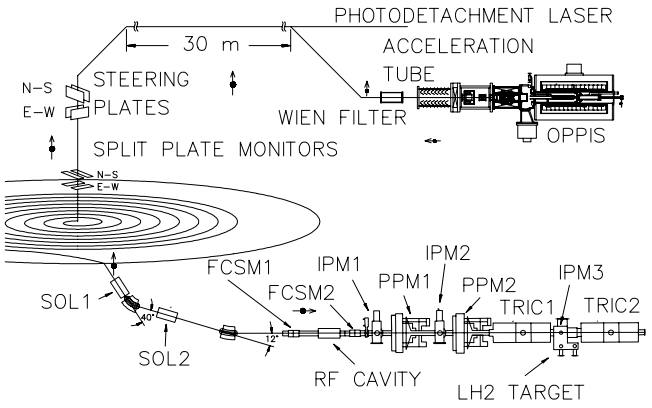

FIG. 2. General layout of the TRIUMF parity experiment. (OPPIS—optically pumped polarized ion source; SOL—spin precession solenoid; FCSM—ferrite cored steering magnet; IPM—intensity profile monitor; PPM—polarization profile monitor; TRIC—transverse field ionization chamber)

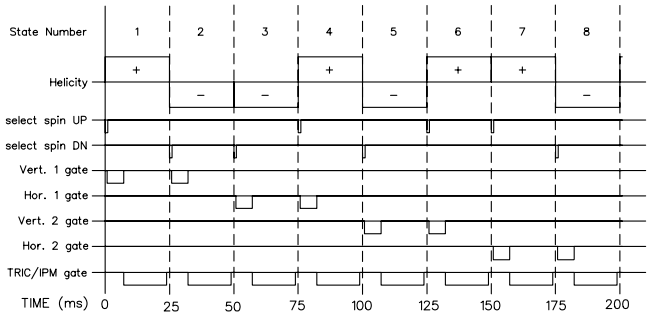

FIG. 3. Sequence of events in one 200 ms, eight-state cycle. Each state starts with a PPM scan. In the first two states of an octet, PPM1 scans vertically, on the next two states, PPM1 scans horizontally. This four-state sequence is then repeated with PPM2.

In the last section of the beam line, the longitudinally polarized beam first passed through a series of diagnostic devices—two beam intensity profile monitors (IPMs) and two transverse polarization profile monitors (PPMs)—before reaching the LH_2 (liquid hydrogen) target, which was preceded and followed by transverse electric field, parallel plate ionization chambers (TRICs) to measure the target transmission. A third IPM was located immediately in front of the LH_2 target, inside the cryostat vacuum.

B. Optically pumped ion source

In the ion source, 9 W of 795-nm laser light was used to optically pump a rubidium vapor whose polarization was ultimately transferred to the protons of the H^- beam. The polarization was reversed using small tilting etalons to make rapid frequency adjustments to the two pumping lasers to match either the σ^+ or σ^- component of the rubidium D_1 transition; the two are separated by 93.5 GHz. No macroscopic electric or magnetic fields were altered. This minimized helicity-correlated changes in accelerated beam parameters other than polarization. This was very important to the success of the experiment. The ion source is the ultimate origin of all helicity-correlated modulations, and the more the unwanted modulations could be reduced at the source the less corrections were required later. The extracted beam current required by the experiment was not large (200 nA) so, to reduce unwanted helicity-correlated modulations, it was possible to sacrifice most of the OPPIS intensity in return for beam quality. For example, the rf bunchers in the injection beam line, which enhance the cyclotron transmission by a factor of 5, also amplify the coherent energy modulations by two orders of magnitude, and could not be used during the parity experiment. High-current OPPIS development [14–16] for high-energy accelerators proceeded at the same time as development of the TRIUMF source and contributed greatly to the parity-violation experiment.

The polarization of the rubidium vapor was monitored and controlled on line by observing the Faraday rotation of light from an additional 100-mW, TiS probe laser that emitted 780.8 nm light—close to the D_2 transition of rubidium. The polarization of the linearly polarized probe laser light rotated through an angle proportional to the rubidium vapor polarization. The Faraday measurements also provided confirmation of the helicity state of OPPIS. The Faraday rotation signal was encoded as a frequency to prevent helicity-correlated signals from being present in the electronics racks. Details of the OPPIS Faraday rotation system are described elsewhere [17].

Every effort was made to tune OPPIS for minimum intensity change on spin flip. The main technique used to do this was to keep the rubidium polarization, as measured by the Faraday rotation, close to 100% and with the two spin states matched to better than $\pm 0.5\%$. It was not possible to eliminate helicity-correlated current modulation completely, but under normal data taking conditions, helicity-correlated current modulations $\Delta I/I=(I^+-I^-)/(I^++I^-)$ of a few parts in 10^5 were routinely achieved.

To enable measurement of the sensitivity of the experiment to coherent intensity modulation, provision was made at the ion source to produce an intentional, controlled, intensity modulation when desired. This was done using an auxiliary 18-W green argon laser (Spectra Physics Inc., operating on all lines with most power at 514 nm and 488 nm) beam that co-propagated with the H^- beam along the 30-m-long horizontal section of the injection beam line, neutralizing through photodetachment a small fraction of the beam. The photodetachment laser could be interrupted synchronously with the parity spin sequence, so that the beam current in every other ''spin off'' (i.e., with the optical pumping lasers blocked with a shutter) data taking cycle was modulated at the 0.1% level.

C. Cyclotron and beam line

1. Beam transport

After extraction from OPPIS, the H^- beam passed through a Wien filter that was tuned to produce vertical polarization at the entrance to the cyclotron. The injection line from the ion source to the cyclotron used electrostatic elements and was magnetically shielded from the fringe field of the cyclotron. Instabilities in the polarized ion source, beam line power supplies, and mechanical vibrations of the whole injector building structure, cause the beam position at the injection point to fluctuate. These fluctuations are converted to energy and current modulations of the accelerated beam. These were significantly reduced by a position stabilization feedback system installed in the vertical section of the injection beam line [18]. The system was based on two split plate beam position monitors, with correction voltages applied to electrostatic steering plates. About 50% of the beam was lost on the split-plates, but the result was a significant improvement in the beam stability and a reduction in noise. The sampling rate of the integrated current feedback amplifier was 1 kHz, so spin-flip correlated position modulations produced in the source at 40 Hz were also reduced by the position stabilization system.

After injection into the cyclotron, the beam was accelerated to 221.3 MeV in the cyclotron and was extracted by a thin stripping foil. Various stripping foil designs were tried, but most of the data were taken with a 2.5 mm wide $\times 26$ mm high$\times 5$ mg/cm^2 thick, pyrolytic graphite foil. This foil was mounted in a special ''bow-saw'' shaped holder that supported the foil from both ends to prevent curling. Following extraction from the cyclotron, the proton polarization vector was precessed through $\pm\sim 63°$ in the first solenoid, 88.61° in the first (40°) dipole, $\pm\sim 87°$ in the second solenoid, and 26.58° in the final (12°) dipole, resulting in a longitudinally polarized beam that was transported to the parity apparatus. The sign of the solenoid rotation was chosen depending on the desired helicity of the tune and the exact solenoid strengths were fine tuned empirically to produce pure longitudinal polarization in the presence of the cyclotron fringe field. In contrast with systems using only one solenoid and one dipole, which can produce longitudinal polarization only at one energy, the TRIUMF system is ca-

TABLE I. Beam energy measurements made during the three running periods. The uncertainties shown are statistical only. The absolute calibration of the BEM is known to be ± 0.23 MeV.

Running period	Beam energy (MeV)
1997	221.30 ± 0.03
1998	221.5 ± 0.1
1999	221.3 ± 0.1

pable of producing longitudinal polarization at any proton energy up to 500 MeV [19].

Ideally, the beam transport should produce an achromatic waist downstream of the LH_2 target, to minimize the effect of first moments of transverse polarization, which are the dominant source of systematic error in this experiment, as they couple to the large (~ 0.3) parity allowed transverse analyzing power A_y. The rotation of phase space introduced by the superconducting solenoid magnets was approximately compensated for by rotating the quadrupole doublet before the final 12° bend by 37.4° and the quadrupole triplet following the bend by 17.2°. To reverse the spin direction at the parity target relative to the spin in the cyclotron, the directions of the solenoidal fields and the signs of the quadrupole rotations were reversed. In principle, that should have been all that was required. In practice, small adjustments to some quadrupole and steering magnets were necessary, but empirical tunes were developed that kept these changes very small (1%–2%).

Between the second solenoid magnet and the final 12° bend, where the polarization of the beam has both a longitudinal and a sideways component, a four branch polarimeter [20] was used to measure the transverse polarization components at regular intervals. Since the angle of the polarization vector is known at this location, the absolute beam polarization could be determined. Once the beam passed the final dipole magnet, the polarization was longitudinal and the PPMs determined the small transverse components. The upstream polarimeter was also used, with purely vertically polarized beam, to check the absolute calibration of the PPMs.

Just after the upstream polarimeter, a beam energy monitor (BEM) [21] was available to measure the energy of the proton beam. The BEM achieves a statistical precision of ± 20 keV in ≈ 1 h. The absolute calibration is known to be ± 230 keV [22]. The (BEM) target could not be inserted during normal data taking, so periodic BEM measures were made to check the beam energy. Table I summarizes the beam energy measurements.

2. Beam energy

The beam energy of 221.3 MeV at the target entrance was chosen so that the $(^1S_0\text{-}^3P_0)$ contribution would be zero when the acceptance of the detectors and the energy loss in the target was taken into account. This was done using a Monte Carlo program that simulated the experiment using detailed target and detector geometries, and including the energy dependence of the strong pp phase shifts. It was found that the beam energy was not overly critical; a departure of 1 MeV from the energy for which the $(^1S_0\text{-}^3P_0)$ contribution integrated to zero caused this mixing to contribute only $\sim 10^{-9}$ to A_z. Theoretical calculations of A_z based on total cross section, and which assume no energy loss in the target, show the $(^1S_0\text{-}^3P_0)$ zero at 225 MeV, where the $^1S_0$ and $^3P_0$ strong phase shifts are equal and opposite [23]. According to the Monte Carlo simulation, this theoretical A_z at 225 MeV should be compared to the TRIUMF A_z multiplied by 1.02 ± 0.02.

D. Specialized instrumentation

1. General

Very strict constraints had to be imposed on the incident longitudinally polarized beam to limit both random and helicity-correlated modulations of the beam intensity, energy, horizontal (x) and vertical (y) position and direction, beamwidth (σ_x and σ_y), transverse polarization (P_x and P_y), and first moments of transverse polarization ($\langle xP_y \rangle$ and $\langle yP_x \rangle$). The approach followed was to design the experimental apparatus for minimum sensitivity to beam property variations, to monitor helicity-correlated beam properties during data taking, and to correct the data for all significant helicity-correlated effects. A program of auxiliary calibration measurements was interwoven in the regular data taking cycle in order to establish the sensitivity of the apparatus to all measurable systematic effects under data taking conditions.

The custom-built parity instrumentation occupied approximately the last 10 m of the beam line, between the last quadrupole magnet and the west wall in the TRIUMF proton hall (beam line 4*A*/2). Transverse field parallel plate ion chambers TRIC1 and TRIC2 measured the beam current incident on and transmitted through the target. The parity-violation signal was derived from the helicity-correlated analog signal difference between the beam currents measured by the two TRICs. Upstream of the target were two PPMs to measure the distributions of transverse polarization $P_y(x)$ and $P_x(y)$ across the beam. The three IPMs measured the intensity distribution of beam current in x and y. Two of the IPMs were coupled to a pair of fast ferrite cored steering magnets (FCSMs) that locked the beam path on the desired axis through the equipment.

2. Intensity profile monitors

The IPM signals were based on secondary emission from thin nickel foil strips arranged in harps placed between 8-μm-thick aluminum foils. (A very similar, earlier version is described in Refs. [24,25]). For IPM1 and IPM2 the nickel strips were 3 μm thick, 1.5 mm wide, and spaced 2.0 mm center to center. In IPM3, the nickel strips were 10 μm thick, 2.5 mm wide, and spaced 3.0 mm center to center. Each IPM contained a vertical and a horizontal harp with 31 strips per harp. IPM1 also contained an aluminum normalization foil that provided a beam current signal to the liquid hydrogen target controller. The 31 signals from the strips of each of the six planes were individually amplified and digitized to provide the beam intensity profiles in each spin state. Hardware beam centroid evaluators delivered signals proportional to

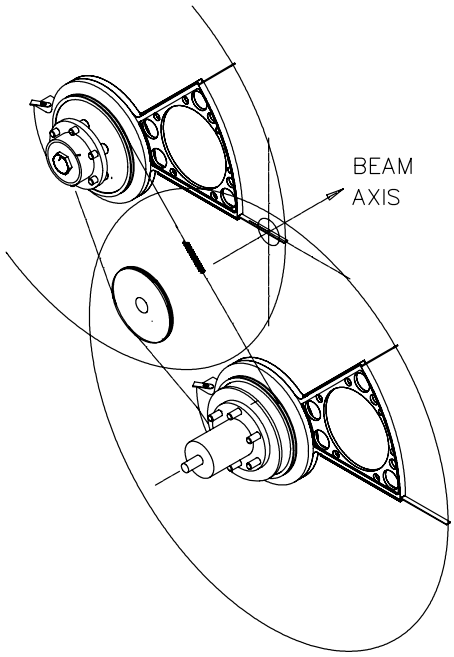

FIG. 4. Method of scanning the CH_2 blades through the beam. The blades measure 5×1.6 mm^2 in cross section and extend 85 mm beyond the holders. Each PPM has two horizontally scanning and two vertically scanning blades. This figure shows a blade at the middle of a vertical scan.

the beam centroids. Corresponding correction signals were used to drive feedback loops to the pair of horizontal and vertical fast FCSMs (Fig. 2). This allowed the beam intensity profile centroids to be kept within ±1 μm with a dc offset less than 50 μm from the desired axis. Sensitivities to helicity-correlated position and size modulations were determined with the beam unpolarized and with enhanced modulations introduced using the fast FCSMs synchronized to the spin sequence.

3. Polarization profile monitors

The PPMs are described in detail in Ref. [26]. Each PPM has four high density polyethylene (CH_2) blades, 5×1.6 mm^2 in cross section. The blades were mounted on wheels rotating at 5 rps, and were scanned through the beam as shown in Fig. 4, two blades scanning vertically through the beam and two blades scanning horizontally. The figure shows one blade in the middle of a vertical scan. Protons elastically scattered from hydrogen in the blades were detected by sets of forward and recoil scintillator telescopes, the geometry of which was set to select only $\vec{p}p$ elastic events at 17.5° laboratory angle, near the maximum in the parity allowed analyzing power A_y. During vertical scans the up-down asymmetry was measured and during horizontal scans the left-right asymmetry was measured. Information from each blade was stored in 80 time bins of 80 μs each, for a total time window of 6.4 ms per blade. As the radius of rotation is 215 mm, this corresponds to $(6.4/200)(2\pi)\times(215)$ mm$=43$ mm centered on the nominal beam axis. From the up-down or left-right asymmetry in each bin, a distribution of transverse polarization across the beam profile was generated. The two PPMs were operated with a 180° angular mismatch, producing eight equally spaced profiles in 1/5 s, or 40 profiles per second. (This is also the spin-flip rate—see Fig. 3.)

The master clock for sequencing the whole experiment, including helicity changes, was derived from 2500-line optical encoders mounted on the PPM drive shafts. Each shaft encoder produced two 2500 cycles per revolution square waves in phase quadrature, permitting the direction of rotation to be determined from whether one signal was high or low at the positive going transition of the other. By recording both the rising and falling edges of both quadrature signals, the PPM control electronics obtained an effective resolution of $4\times2500=10\,000$ lines. The rotation of the two PPMs was synchronized by electronic gearing using position information provided by the shaft encoders. During steady state rotation at 5 rps, the servo system was able to control the angle between the two PPMs to ±3 mrad, corresponding to one-third of the 1.6 mm target blade thickness at the location of the proton beam.

4. Liquid hydrogen target

The LH_2 target had a flask 0.10 m in diameter and 0.40 m long. The target scattered $\sim4\%$ of the beam. It was important that the windows on the hydrogen volume be flat and parallel to prevent motion of the proton beam from creating intensity noise. The hydrogen was contained by 25-μm-thick stainless steel windows. Upstream and downstream of these inside the vacuum vessel were two helium filled chambers, 21 mm thick on the upstream side and 10 mm thick on the downstream side, ensuring that the inner windows were flat. The outer windows of the helium cells were 50-μm-thick stainless steel. The cryostat vacuum vessel was sealed with 25-μm-thick copper windows.

Although a thick target is desirable from the standpoint of increasing the signal, it was also very important that the tails of the beam profile be well contained in the 150×150 mm^2 aperture of the detectors; beam blow-up due to multiple Coulomb scattering limited the target flask length, as well as the thickness of various entrance and exit windows and the thickness of the upstream IPM foils. With the target full, the beam size increased from ≈4 mm (σ of projected profile) at the center of the upstream detector to 15 mm at the center of the downstream detector, and 22 mm by its exit.

Rapid circulation (5 L/s) of the LH_2 reduced density gradients and prevented boiling. A feedback loop using fast and slow heaters controlled the target temperature. The fast heater responded to a beam current signal from IPM1 (Sec. III D 2) and kept the heat load essentially constant when the beam current changed. The slow heater made fine adjustments to hold the LH_2 temperature at 19.3 K to within ±0.2 K over a several week data taking period.

5. Transverse field ionization chambers

Each TRIC (a smaller earlier version is described in Ref. [27]) consisted of a cylindrical enclosure filled with 750 L of ultrahigh purity hydrogen gas at a pressure of about 150 Torr,

and contained an upper cathode plate operated at -8 kV, and a grounded lower signal plate. The TRICs also contained field shaping electrodes plus guard rings to ensure a uniform sense region, 150 mm wide$\times$150 mm high$\times$600 mm long between the parallel electrodes. High-Z, low-energy spallation products from the chamber windows can cause large fluctuations in the signal, so the entrance and exit windows were located $\approx$900 mm from the center to prevent spallation products from entering the active region. Other considerations in the design of the TRICs were noise due to delta ray (δ-ray) production and ion pair recombination. Recombination is reduced by lower gas pressure and higher voltage, both of which reduce the space charge density in the active volume. In practice, compromises must be made because too high a voltage causes increased noise from corona discharge and low pressure reduces the desired signal. δ-rays are electrons produced by collisions of the protons with the detector gas. The δ-ray signal is noisy, and the major contribution to this signal is from δ-rays at large angles. The transverse dimension of the ion chamber was a trade off between a small transverse size which would minimize δ-ray noise and a large transverse dimension which accepts all the beam. The 150-mm transverse dimension was the smallest that gave an acceptably low sensitivity to beam size modulation based on simulations. The main signal from the proton beam increases with the length of the active region. This was limited by the available space in the beam line; 600 mm was the longest practical length.

The noise in the ion chamber signals has two incoherent contributions—shot noise from the statistical nature of the proton beam and noise contributed by the chamber itself. The noise figure α expresses the chamber noise as a fraction of the shot noise. When the difference between the upstream and downstream chambers is taken, most of the shot noise contribution disappears because, except for the 4% scattered by the target, each upstream proton also passes through the downstream chamber. The chamber noise, on the other hand, does not cancel, and the running time is dominated by chamber noise. In this experiment the counting time was $\approx$15 times that which would have been expected from counting statistics alone. The fact that the run time was dominated by chamber noise resulted in the seemingly paradoxical result that better precision was obtained by lowering the beam current, because this reduced the detector noise figure. In a series of test runs at progressively reduced beam currents, the A_z distribution became narrower until $\approx$100 nA. The 200 nA selected for running was a compromise between lower current for better precision on A_z and higher current for better precision from the PPMs, which *were* limited by counting statistics.

IV. DATA ACQUISITION

The data were taken in $\frac{1}{5}$ s (200 ms) cycles, each cycle consisting of eight $\frac{1}{40}$ s (25 ms) spin states arranged in the pattern $(+--+-++-)$ or $(-++-+--+)$. This pattern makes the result insensitive to linear or quadratic drifts. The cycles were further arranged in an eight cycle (64 spin state) ''supercycle,'' with the starting state of each cycle following the same $(+--+-++-)$ or $(-++-+--+)$ pattern. The initial spin state of each supercycle was chosen at random. In the frequency domain, this switching pattern contains odd multiples of 5 Hz, with the largest harmonic content at 15-Hz. The data acquisition produced online values for the amplitude and phase of the dominant 15 Hz component. This was derived from a 16 spin-state cycle. The 64 spin-state supercycle gave the option of using more advanced digital filtering schemes on the difference signal, but these were only used during early development runs. Twenty percent of the data were taken with all the spin-flipping equipment running, but with the pumping lasers blocked with a shutter to guarantee zero polarization. In addition, as mentioned earlier, half of these spin off data were taken with an artificially enhanced intensity modulation synchronized with the spin flip.

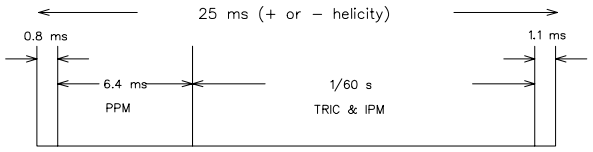

FIG. 5. The timing of detector readout intervals within one spin state. The initial 0.8 ms allows for ion source settling time. The 6.4-ms PPM interval corresponds to a 43-mm scan centered on the beam axis. The TRIC interval was 1/60 s to eliminate sensitivity to 60 Hz or harmonics of 60 Hz.

As shown in Fig. 5, each 25-ms spin state was divided into polarization measuring and asymmetry measuring intervals. Following a short dead time to allow the mechanical etalons which change the ion source spin-state time to stabilize, was a 6.4-ms window during which one of the eight blades of the scanning polarimeters passed through the beam. The TRIC and IPM signals were then integrated over exactly 1/60 s to eliminate sensitivity to 60 Hz or harmonics of 60 Hz. The dead interval at the end of each state was intended as a buffer to absorb any timing jitter due to imperfect rotation speed of the PPMs. As it turned out, the timing jitter was less than 0.1 ms and this buffer zone was more than adequate.

The minimum dataset for which a full set of helicity-correlated beam properties could be extracted was a 0.4 s ''event pair'' corresponding to two full 360° rotations of the PPMs, as this gave both spin states for each PPM blade.

As noted in the ion source section, the spin state was transmitted as a frequency to prevent coupling the spin-flip signal into the data acquisition. The effectiveness of this isolation was checked by running the complete data acquisition system including the ion source, but with detector signals supplied by a battery. False A_z from electronic cross talk was found to be less than 4×10^{-9}, an upper limit determined by the statistics of the test (cross talk was probably less).

The rotation speed of the PPMs is locked to a signal derived from the zero crossing of the 60-Hz ac line. Since 0.2 s taken for one PPM rotation is exactly 12 cycles of the 60-Hz line, one would expect a given PPM blade to always pass through the beam at the same phase of the ac line. To prevent this, a small controlled phase slip was introduced. The rate of slip was programmable. For data taking it was set for one

complete cycle of the 60-Hz line in 18 min. Although the phase of one PPM relative to the other is ''quantized'' by the finite resolution of the encoders, the angular frequency of rotation is not, and in principle can be locked to a square wave of any frequency. In practice, roundoff error in the motor control computer limited the choices of the reference frequency. The 18 min for 360° of slip corresponded to one of the acceptable values.

In addition to the regular data taking runs, many dedicated control measurements were made to measure the sensitivity of the apparatus to helicity-correlated beam properties, specifically: position, size, intensity, transverse polarization, and energy modulation at the ion source.

V. THE DATA

A. Raw dataset

The parity data used in the final analysis were acquired during three major data taking periods—February-March 1997, July-August 1998, and May-June 1999. The data were recorded as a series of ''runs'' of ≈ 1 h each. Statistics for the combined set are the following:

(a) 3.8×10^6 event pairs, (b) 375 runs in positive beam line helicity, (c) 368 runs in negative beam line helicity, (d) 80 position modulation runs, (e) 81 size modulation runs, (f) 40 energy modulation runs, and (g) 109 neutral axis scans.

The runs were grouped into 23 sets, a new set being started following each retune of the beam line (usually involving a reversal of the helicity at the parity apparatus relative to the ion source).

B. Reduced dataset

During data taking every effort was made to maintain the optimum beam conditions (quiet beam, good longitudinal polarization, low transverse polarization, low first moments of transverse polarization, beam on axis, stable position and size, low intensity modulation) and to stop data taking to correct the beam and cyclotron tune when these conditions were not met. Nevertheless, some data were recorded for which conditions were not ideal. The raw data sample was therefore subjected to data quality cuts prior to inclusion in the final analysis.

The data quality cuts were conservatively chosen to ensure that corrections to the reduced dataset based on critical helicity-correlated beam parameters would be consistent with sensitivities measured in ancillary calibration experiments. The data quality cuts first eliminated 46 data runs for which the TRIC difference signal was anomalously noisy, indicating unstable beam conditions. They also eliminated any data for which diagnostic monitor outputs could be considered spurious. The cuts used are summarized in Table II. There were both ''hard cuts'' at a fixed value of beam parameter and ''soft cuts'' at $\pm 3\sigma$ from the mean value. The entire data reduction process reduced the size of the total set by 30%, but significantly improved the quality of the data sample. χ^2_ν for the uncorrected data of the 23 sets went from 11.3 per degree of freedom before the cuts were made to 5.5 after the cuts. It is important to emphasize that the approach used to determine the sensitivity to intrinsic polarization moments, which was the dominant systematic error correction, required consistent and stable beam conditions—in particular, the ratio of beam sizes at IPM1/IPM2 and the ratio of intrinsic polarization moments at PPM1/PPM2 must be constant over the data sample used to determine the sensitivities, or the method is invalid.

TABLE II. Summary of data reduction cuts. Except for the beam intensity, the center of the acceptance window for each parameter is the measured centroid of that beam parameter's distribution. The hard cuts are wide enough to include at least four standard deviations.

Beam parameter	Acceptance window
Neutral axis x,y	± 0.3 mm
Position	$\pm 3\sigma$ (soft)
Width	± 1.0 mm
Skew	± 0.2 mm
Intensity	196–204 nA
Intrinsic moments	± 3.0 mm

It is important to emphasize that no data cuts were applied to the parity-violating asymmetry A_z itself. The ultimate test of the consistency and validity of the data analysis and corrections procedure is the quality of the corrected dataset shown in Fig. 6. The top panel in Fig. 6 shows the results for the reduced dataset, before corrections were made for systematic errors. The bottom panel shows the corrected results from which the final A_z was obtained. This corrected dataset was subjected to a regression analysis in which residual sensitivities to helicity-correlated beam parameters were explored. No statistically significant residual sensitivities were found, lending confidence to the interpretation of the results. Details of the corrections procedure are given in the following sections.

VI. SOURCES OF ERROR

Sources of error can be divided into those that are related to the beam helicity and those that are not. Beam property changes that are synchronized with spin flip (''coherent'' or ''helicity-correlated'' changes) can shift the centroid of the A_z distribution and cause a false signal of parity-violation. Changes that are not helicity-correlated, such as detector noise and random variation in beam properties, do not bias the result, but they increase the run time required to reach a given precision.

A. Random changes

The ultimate limit to the statistical precision of the experiment was set by the counting statistics of the scattered protons. For a target scattering 4% of the 200-nA beam, the rate of scattered protons is 50 GHz, which would make it possible to measure A_z to $\pm 0.2 \times 10^{-7}$ in 20 h if individual scattered protons could be counted. However, 50 GHz was too high for direct counting, and so current mode detection was used. As noted already in the ion chamber section, the

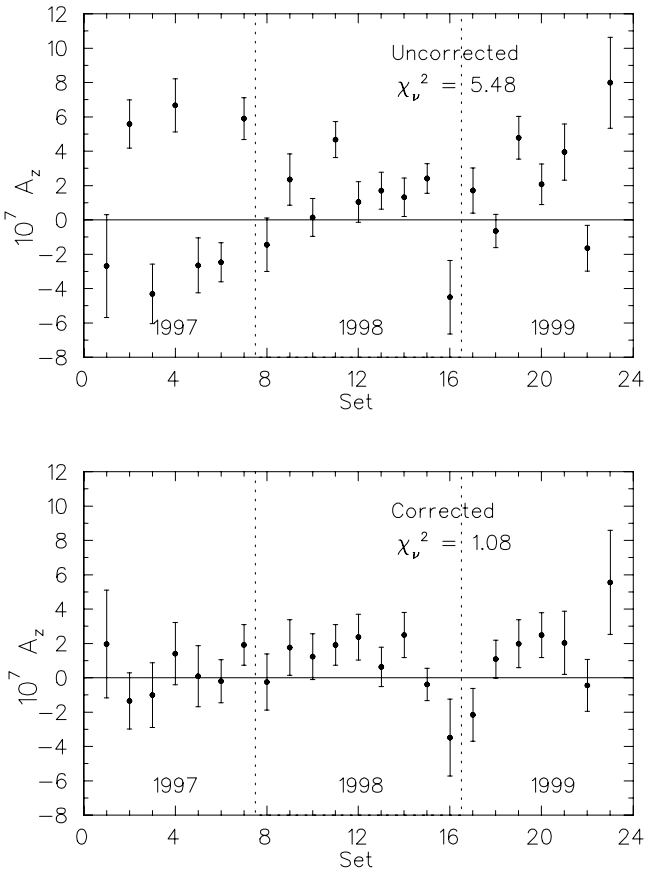

FIG. 6. E497 results before and after correction. The data are divided into 23 sets of alternating beam line tune. The top panel shows the results after beam quality cuts, but before the data were corrected for systematic errors. The bottom panel shows the data after correction. The error bars in the bottom panel are slightly larger due to uncertainties in the corrections.

counting time was dominated by detector noise. Other random variations in beam properties such as intensity and position also contributed noise and further increased the required run time. It proved to be a net advantage to devote significant beam development time to producing quiet, stable, beam.

B. Helicity-correlated changes

The approach to minimizing and correcting for the false A_z signal due to helicity-correlated beam property changes was as follows.

(a) Careful design and operation of the TRIUMF optically pumped polarized ion source and cyclotron made it possible to change the spin direction with very little effect on the other beam properties. (b) The design of the parity equipment and the operating conditions of the experiment were carefully chosen to minimize the sensitivity to helicity-correlated changes. (c) Calibration runs determined the sensitivity to helicity-correlated modulations. (d) The beam properties were continuously monitored during data taking so the actual helicity-correlated changes were known, and appropriate corrections were applied.

VII. CORRECTION FOR SYSTEMATIC ERRORS

The effects of modulations in beam intensity, position, size, transverse polarization, and energy were considered.

Measurements made early in the experimental program revealed significant correlations between beam parameters. For example, horizontal and vertical beam motion are often highly correlated. To be sure of extracting the correct sensitivities, separate control measurements were made in which each beam property in turn was artificially modulated, and the effect on apparent A_z was recorded. The sensitivities obtained by this method were consistent with sensitivities extracted by multilinear regression using the natural variation of beam parameters. Most importantly, the regression analysis showed no significant sensitivity to *products* of beam modulations, so the false A_z was the sum of the contributions of the individual coherent modulations.

For the sensitivity calibrations made by varying one parameter at a time, measurements were made using modulations of different size and sign. The false asymmetry was linear in the modulation, passing through zero at zero modulation. To determine the sensitivities used for data reduction, large values of modulation were used to give accurate results in a short time. To determine the sensitivity to first moments of transverse polarization, which gave the largest false asymmetry, much larger transverse polarizations were used for calibration than were present in the parity beam. This was justifiable because false asymmetries must be linear in polarization, and the use of large polarizations allowed the displacements needed for the calibration to be reduced. The measured false asymmetry was linear in polarization moment.

A. Coherent intensity modulation (CIM)

As the energy of the beam was 27 MeV lower at TRIC2 than at TRIC1, the TRIC2 gas pressure was lowered relative to TRIC1 to equalize ion chamber currents. A hardware gain on the TRIC1 signal was then adjusted to minimize common-mode noise in the amplified difference signal, $1000\times(I_2-gI_1)$ which was digitized, where g is the hardware gain; g is very close to unity. The helicity-correlated part of the difference, which should be proportional to A_z, nevertheless, contains a coherent current modulation component due to imperfect common-mode rejection arising from gain mismatch and nonlinearity of the ion chambers. If the current signal from TRIC2 is $I_2^{\pm}=aI_1^{\pm}[1-S(1\pm P_zA_z)]$ then, expressing the difference in current for the two helicity states as $I_1^{\pm}=I_1\pm\delta I_1$, one can define an ''analog asymmetry''

$$\epsilon_a=\frac{(I_2^+-gI_1^+)-(I_2^--gI_1^-)}{2I_1}$$

$$=-SaP_zA_z+\left(aT-g+I_1T\frac{da}{dI_1}\right)\frac{\delta I_1}{I_1}, \qquad (1)$$

where S is the nuclear scattering probability in the LH_2 target ($S\simeq 0.04$) and $T=1-S$. The quantity a is a function of TRIC1 and TRIC2 gas gains, and is nominally equal to $1/T$;

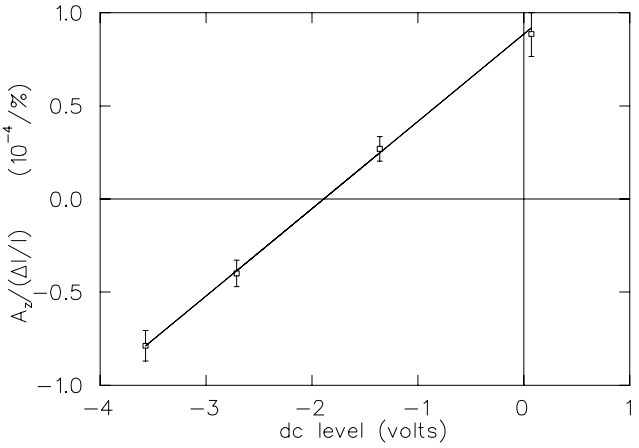

FIG. 7. A scan of the subtractor box settings taken during the July 1998 running period. The plot shows the sensitivity to CIM as a function of the subtractor box dc level. The dc level is a sensitive indication of the setting of the fine gain control; a fractional gain change of 10^{-4} causes a shift of 0.7 V in the dc level. This particular scan gave an ideal dc level of -1.9 V for zero sensitivity to CIM.

it was adjusted with TRIC2 gas pressure. The hardware gain g was set by zeroing the false parity signal when the beam current was modulated by the photodetachment laser. Because of the nonlinearity term, g must be reset if the beam current changes.

A beam current stabilization system was implemented which restricted beam current excursions to the range 200 ± 2 nA [18]. The current stabilization system took a current signal from the upstream ionization chamber (TRIC1) and fed a correction voltage to an electrostatic quadrupole lens just upstream of a set of slits in the injection line. The injection line was tuned with a slight excess of current so that, at the set point, about 10% of the beam was skimmed by the slits. To exclude coupling of current modulation to position and energy modulations, the sampling rate was slow (0.5 Hz), much slower than the spin-flip rate of 40 Hz. The active range of the current stabilization loop was quite low ($\pm 10\%$) to avoid correcting drifts caused by large excursions of cyclotron tune. The current loop operation was a sensitive indicator of cyclotron stability, and operators made adjustments to the cyclotron tune when necessary. Even under conditions of constant beam current, periodic adjustments of g were needed to compensate for small drifts in the ion chamber gains. The setting for best common-mode rejection was checked periodically by turning on the photodetachment laser, creating a ($\sim 0.1\%$) coherent intensity modulation, and performing a scan of subtractor box settings. The results of such a calibration are shown in Fig. 7. Because the difference signal was multiplied by 1000, the dc level was a sensitive indication of the setting of the hardware fine gain. A fractional change of 10^{-4} in the hardware fine gain caused a dc shift of 0.7 V in the subtractor box output.

During data taking, CIM was measured continuously by the ion chamber (TRIC1) upstream of the target. As noted in Sec. III B, this was normally less than a few parts in 10^5. Because the sensitivity to CIM changed between the dedicated CIM runs used to reset the subtractor box, the sensitivity to CIM was also measured during data taking. Periods of enhanced (0.1%) coherent intensity modulation were interleaved with the main data. A typical sensitivity was $A_z^{false}=(1.6\times 10^{-4})(I_b-200)(\delta I/I)$, where I_b is the beam current in nanoamperes. Table III shows the average sensitivities to coherent intensity modulation for the different running periods and Fig. 8 shows a histogram of the sensitivities for a typical (~ 1 h) run.

TABLE III. Average sensitivities to coherent intensity modulation. The sensitivities are determined from all CIM data with $|\Delta I/I| \geqslant 0.06\%$.

Set	Sensitivity $(10^{-7}/\%)$	CIM events
1997	36 ± 19	83 636
1998	138 ± 8	106 520
1999	73 ± 11	90 955

B. Coherent position modulation

Coherent position modulation was measured by two of the three IPMs. During the 1997 running period, IPM1 and IPM3 were used because their separation was greater and, all else being equal, position control should have been better. Unfortunately, IPM3 picked up noise from the liquid hydrogen target circulation fan, so for the 1998 and 1999 data, IPM1 and IPM2, located 1.8 m apart along the beam line, were used. Using two IPMs permits measuring both tilts and parallel shifts of the beam. The measured coherent modulations are shown in Tables IV and V. The sensitivity to beam motion was measured in separate control measurements during which the beam position was modulated in a variety of ways using the FCSMs.

The false analyzing power arising from helicity-correlated beam position was parametrized as

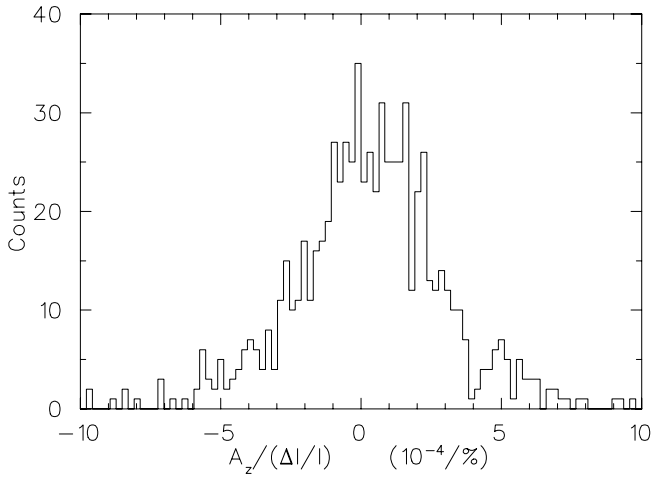

FIG. 8. CIM data for a typical 1 h run. The plot shows a histogram of the sensitivity to $\delta I/I$. Data have been excluded for which $|\delta I/I|<0.06\%$. The mean is 0.23 and the standard deviation 2.6, in units of $(10^{-4}/\%)$.

TABLE IV. Summary of position and size modulation for the 1997 dataset. These data used IPM3 for fast position control. Changing the Wien filter sets the spin direction in the cyclotron relative to the ion source and the beam line sets the helicity at the parity apparatus relative to the cyclotron.

	Wien filter +		Wien filter −	
Beam line	+	−	+	−
$\Delta\sigma_{x_1}$ (nm)	119±49	−137±43	−101±59	8±48
$\Delta\sigma_{x_3}$ (nm)	65±79	−156±76	−110±118	−45±91
$\Delta\sigma_{y_1}$ (nm)	126±44	−212±44	−36±54	41±45
$\Delta\sigma_{y_3}$ (nm)	81±75	−200±72	−54±116	−11±84
Δx_1 (nm)	5±33	19±28	−34±40	38±36
Δx_3 (nm)	−30±34	−40±34	10±46	4±37
Δy_1 (nm)	−46±26	89±27	−7±33	−10±27
Δy_3 (nm)	−27±36	−12±33	24±55	−78±43

$$\Delta A_z = \left(\frac{\Delta x_1 + \Delta x_2}{2}\right)(a_x x_1 + b_x x_2 + c_x) + \left(\frac{\Delta x_1 - \Delta x_2}{2}\right)(d_x x_1 + e_x x_2 + f_x) + \left(\frac{\Delta y_1 + \Delta y_2}{2}\right)(a_y y_1 + b_y y_2 + c_y) + \left(\frac{\Delta y_1 - \Delta y_2}{2}\right)(d_y y_1 + e_y y_2 + f_y), \quad (2)$$

where Δx and Δy are the horizontal and vertical helicity-correlated beam motion, x and y are the beam position and the 1 and 2 subscripts refer to IPM1 and IPM2. The parameters a–f were extracted from a fit to the calibration data. Details may be found in Ref. [11]. Figure 9 shows the results of such a fit. The abscissa shows the false asymmetry predicted using Eq. (2) with the fitted parameters and the ordinate shows the false asymmetry actually measured with the calibration data.

C. Coherent beam size modulation

Coherent beam size modulation was also measured by the two IPMs, and the observed values are listed in Tables IV and V. The sensitivity to beam size was determined by control measurements in which the beam size was intentionally modulated by driving the FCSMs as quadrupoles.

TABLE V. Summary of position and size modulation for the 1998 and 1999 datasets. IPM2 was used for fast position feedback, replacing IPM3. The Wien filter was + for all these data, producing spin up in the cyclotron. The beam line rotates this to + or − helicity at the parity apparatus.

Beam line:	+	−
$\Delta\sigma_{x_1}$ (nm)	−17±38	0±35
$\Delta\sigma_{x_2}$ (nm)	8±8	−35±7
$\Delta\sigma_{y_1}$ (nm)	−6±37	1±35
$\Delta\sigma_{y_2}$ (nm)	17±7	−37±5
Δx_1 (nm)	1±14	−1±6
Δx_2 (nm)	7±11	−9±5
Δy_1 (nm)	17±11	3±8
Δy_2 (nm)	16±10	2±7

The false analyzing power due to beam size modulation was expressed as

$$\Delta A_z = \alpha_x \sigma_{x_1} \Delta\sigma_{x_1} + \beta_x \sigma_{x_2} \Delta\sigma_{x_2} + \alpha_y \sigma_{y_1} \Delta\sigma_{y_1} + \beta_y \sigma_{y_2} \Delta\sigma_{y_2}, \quad (3)$$

where σ is the rms beam size and $\Delta\sigma$ is the helicity-correlated change in beam size. As with position modulation, the parameters were extracted from a fit to the calibration data. Because the quadrupole configuration of the FCSMs caused the beam to be steered somewhat when the size was modulated, correction for position modulation had to be included in the fit. Figure 10 shows the results of a fit to a series of size modulation calibration runs.

D. Transverse polarization

If the proton spin is not perfectly longitudinal, the small transverse component will reverse with helicity. This can couple to the relatively large ($\sim$0.3) parity allowed analyzing power to cause a false parity-violating signal. Figure 11

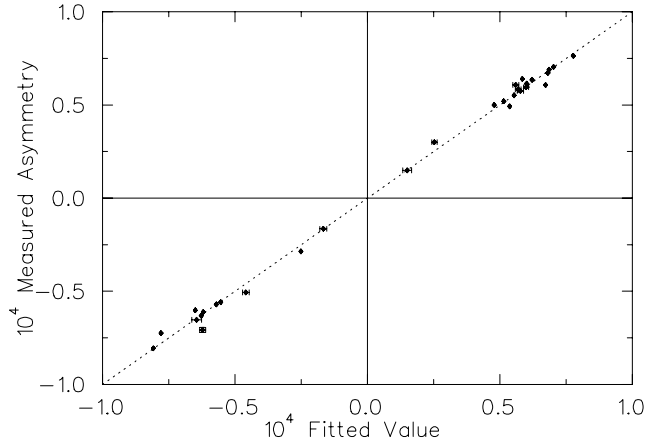

FIG. 9. Calibration of sensitivity to coherent position modulation. The abscissa shows the false asymmetry based on sensitivities extracted from calibration runs and the ordinate shows the asymmetry actually measured.

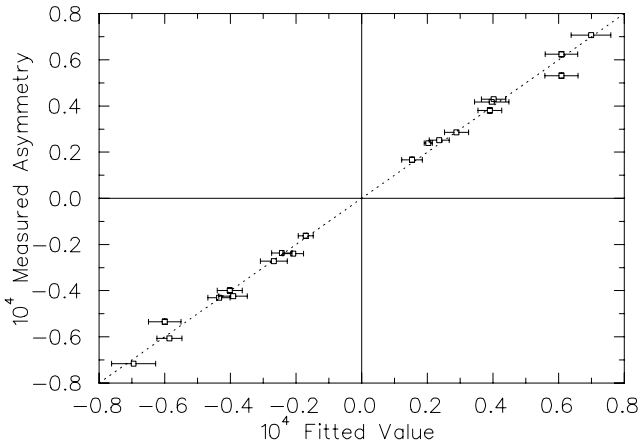

FIG. 10. Calibration of sensitivity to coherent size modulation. The abscissa shows the false asymmetry based on sensitivities extracted from calibration runs and the ordinate shows the asymmetry actually measured.

uses a pencil beam with a vertical transverse polarization to illustrate the mechanism. Because the parity allowed analyzing power is positive, slightly more beam will be scattered to the left in the positive helicity state, and to the right in the negative helicity state. If the beam passes through the center (neutral axis) of the detector, as shown in the left-hand panel, the response will be the same for both helicity states and no false effect arises. If, on the other hand, as shown in the right-hand panel, the beam does not pass through the center of the detector, more signal will be recorded in one helicity state than in the other. To a very good approximation, the effect is found to be proportional to the size of the transverse component multiplied by the distance the beam is off center at the detector—i.e., to the *first moment* $\langle x\rangle\langle P_y\rangle$ of transverse polarization at the detector.

In a field-free region, a real particle beam of finite extent is made up of a bundle of straight rays such as the pencil beam in this example. The first moment for the beam is the linear sum of the first moments of the individual rays. Since

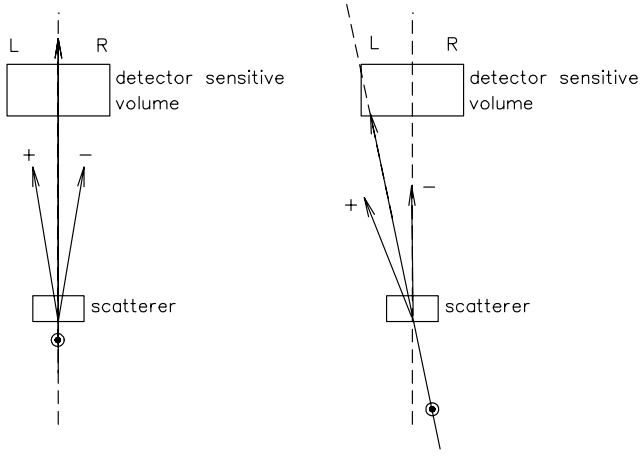

FIG. 11. The effect of transverse components of polarization. The combination of a transverse polarization component with a beam displacement from the neutral axis will cause a false signal of parity violation.

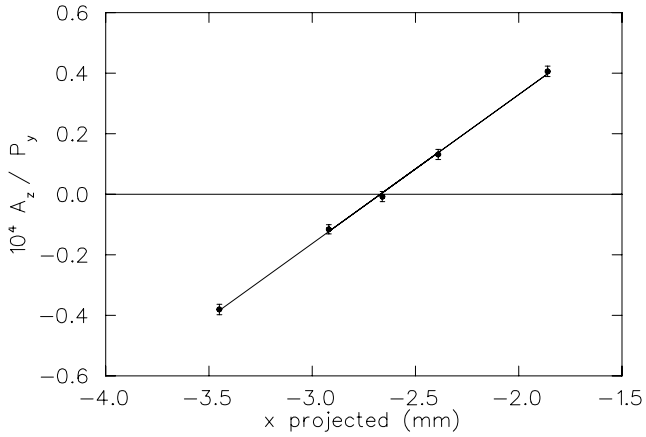

FIG. 12. A horizontal neutral axis scan. A vertically polarized beam ($P_y = 0.76$) was scanned horizontally and the sensitivity to P_y plotted as a function of x projected to the "magic z" (z location where the false A_z does not depend on angle). A beam with $x_{proj} = -2.7$ mm was found to produce no false signal from vertical polarization components.

the first moment for a ray is proportional to the distance of the ray from the zero axis and varies linearly with distance along the beam, changing sign where the ray crosses zero, the first moment for a particle beam will vary linearly with distance along the beam. A real beam can have a substantial first moment of transverse polarization even if the net transverse polarization is zero. In the example of Fig. 11, the vertical polarization could be "up" on the right side of the beam and "down" on the left side.

To determine the first moment sensitivities, test runs were made with pure vertical and pure horizontal polarization. By scanning the vertically polarized beam horizontally it was possible to generate known moments, $\langle x\rangle\langle P_y\rangle$, and by scanning the horizontally polarized beam vertically known $\langle y\rangle\langle P_x\rangle$ moments could be generated. Although in principle the first moments must be known at the two detectors, because first moments vary linearly with distance along the beam line, knowledge of the first moments at *any* two locations is sufficient.

The transverse polarization profiles were measured by the two polarization profile monitors (PPMs in Fig. 2) located 1.8 m apart along the beam line and, for convenience, the first moment sensitivities were expressed in terms of the sensitivities at the PPMs. The first moment scans also defined the beam trajectory for which there was zero sensitivity to average transverse polarization. Such a trajectory was referred to as a *polarization neutral axis*. Polarization neutral axes were determined in both the horizontal and vertical directions and, during data taking, the beam was held on this neutral axis by the servo system. Figure 12 shows an example of a horizontal neutral axis scan. Another consequence of the linear behavior of the first moments with distance z is the presence of a "magic z" downstream of TRIC2. *Any* beam with zero first moment at this z will cause no false effects. Also notice that the measurements shown in Fig. 12 confirm the linear relation between first moment and false A_z.

TABLE VI. Fitted first moment sensitivities from the neutral axis scans.

Sensitivity (10^{-7})	Feb97	Jul98	May99
$a_1(\mu\mathrm{m}^{-1})$	1.91 ± 0.03	1.85 ± 0.01	1.83 ± 0.02
$a_2(\mu\mathrm{m}^{-1})$	-2.47 ± 0.01	-2.47 ± 0.01	-2.44 ± 0.01
$(-a_1y_1^{na}-a_2y_2^{na})$	-0.55 ± 0.01	-1.15 ± 0.01	-0.26 ± 0.01
$b_1(\mu\mathrm{m}^{-1})$	-1.51 ± 0.03	-1.49 ± 0.01	-1.49 ± 0.02
$b_2(\mu\mathrm{m}^{-1})$	2.02 ± 0.04	2.00 ± 0.01	1.98 ± 0.01
$(-b_1x_1^{na}-b_2x_2^{na})$	1.31 ± 0.03	-0.35 ± 0.01	0.50 ± 0.01
χ^2_ν	1.17	1.96	2.05

In analyzing the effect of first moments, *extrinsic* first moments, $\langle x\rangle\langle P_y\rangle$ and $\langle y\rangle\langle P_x\rangle$, caused by a beam which has some net transverse polarization and whose centroid is displaced from the neutral axis, were treated separately from *intrinsic* first moments, $\langle xP_y\rangle$ and $\langle yP_x\rangle$, which do not depend on the position of the beam, but rather arise from the distribution of components within the beam. By holding the beam on the polarization neutral axis it was possible to virtually eliminate corrections for *extrinsic* first moments. *Intrinsic* first moments, on the other hand, are independent of beam position, arise in the cyclotron and beam line, and were very hard to control.

The false asymmetry arising from extrinsic and intrinsic first moments can be written

$$\begin{aligned}\Delta A_z=\langle P_x\rangle[a_1(\langle y_1\rangle-y_1^{na}) &+a_2(\langle y_2\rangle-y_2^{na})\\ +\langle P_y\rangle[b_1(\langle x_1\rangle-x_1^{na}) &+b_2(\langle x_2\rangle-x_2^{na})]\\ +a_1\langle yP_x\rangle_1 &+a_2\langle yP_x\rangle_2\\ +b_1\langle xP_y\rangle_1 &+b_2\langle xP_y\rangle_2,\end{aligned}\tag{4}$$

where the first two lines are the contribution from *extrinsic* first moments and the second two lines are the contribution from *intrinsic* first moments. Note that the first moment sensitivities, a_1, a_2, b_1, and b_2, are identical for intrinsic and extrinsic moments.

The results of the neutral axis scans are shown in Table VI. The quantities $(-a_1y_1^{na}-a_2y_2^{na})$ and $(-b_1x_1^{na}-b_2x_2^{na})$ depend on what axis x and y are measured from. They are zero if x_1, y_1, x_2, and y_2 are measured relative to the neutral axis. One notes that the sensitivities to first moments are very consistent from run period to run period. In units of 10^{-7} $\mu\mathrm{m}^{-1}$, the sensitivity to $\langle y\rangle\langle P_x\rangle$ is 1.8 at PPM1 and -2.5 at PPM2. The sensitivity to $\langle x\rangle\langle P_y\rangle$ is -1.5 at PPM1 and 2.0 at PPM2.

There were no magnetic elements after the first PPM, so the first moments of transverse polarization varied linearly with position along the beam line. Furthermore, for a fixed setting of the upstream beam line magnets, the first moments at PPM1 and PPM2 tended to scale together so that, over a wide range of first moments, the *ratio* of first moments at PPM1 and PPM2 had a constant value. Since the neutral axis scans showed that the first moment sensitivity at PPM1 was of opposite sign to, and 75% of the magnitude of, that at PPM2, if the PPM2 first moment were always 75% of the PPM1 first moment, then the two false effects would cancel, and the *effective* sensitivity to first moments would be zero. This would correspond to a beam whose first moment of transverse polarization goes through zero at the magic z. By adjusting the beam convergence, an attempt was made to achieve this magic moment ratio between PPM1 and PPM2. Unfortunately, the ability of the PPMs to measure this ratio to sufficient precision in a reasonable amount of time was very limited, so the cancellation was not perfect and the residual, effective, first moment sensitivity had to be extracted from the data. This could be done either by regressing the first moment ratio from the data and using the sensitivities measured in the neutral axis scans or by regressing the correlation of A_z with average first moment directly from the data. The two methods agreed with each other, but the latter method produced the smallest statistical spread and was the method used to correct the data.

E. Energy modulation

Since the beam energy in the downstream TRIC was on average 27 MeV lower than in the upstream TRIC due to energy loss in the target, helicity-correlated energy modulation caused a systematic error due to the nonlinear energy dependence of the proton beam energy loss in the hydrogen gas of the TRICs. The sensitivity to coherent energy modulations was determined using an rf accelerating cavity placed upstream of IPM1 in the beam line. The measured sensitivity of false A_z, $(2.9\pm0.3)\times10^{-8}$ eV^{-1}, was in excellent agreement with predictions based on the variation of stopping power with energy.

Energy modulation of the extracted beam was caused by position modulations of the radial intensity distribution at the stripping foil; this converted radial position modulation of the injected beam to energy modulation of the extracted beam. The primary coherent energy modulation produced in the source was converted to position modulation in the injection beam line and then back to energy modulation at the extraction foil. Direct measurements using a magnetic spectrometer (1.2 m dispersion) in another beam line (4B) at TRIUMF showed the energy modulation of the extracted beam to be $\approx$100 to 200 times greater than the energy modulation at OPPIS. During the parity runs this direct measure could not be made, but frequent measures of energy modulation at OPPIS and of dA_z/dE_{oppis} were made. The dA_z/dE_{oppis} sensitivity was measured by applying a square wave voltage of 0.5 V amplitude to the electrically isolated

TABLE VII. Settings of the Wien filter and beam line for the 23 datasets.

Set, (Wien filter, beam line)		
1,(+,+)	9,(+,−)	17,(+,+)
2,(+,−)	10,(+,+)	18,(+,−)
3,(+,+)	11,(+,−)	19,(+,+)
4,(+,−)	12,(+,+)	20,(+,−)
5,(+,+)	13,(+,−)	21,(+,+)
6,(−,+)	14,(+,+)	22,(+,−)
7,(−,−)	15,(+,−)	23,(+,+)
8,(+,+)	16,(+,+)	

sodium ionizer in OPPIS. These dA_z/dE_{oppis} runs were then corrected for all known systematic errors (dominated by dI/I), and it was assumed that the residual false A_z arose from energy modulation of the extracted beam. The residual false A_z was proportional to the energy modulation applied at the source. A comparison of the measured dA_z/dE_{oppis} to the dA_z/dE measured in the beam line with the rf cavity (Sec. VII E) indicated that the cyclotron amplified dE_{oppis} by a factor of about 130, in agreement with the magnetic spectrometer measurements.

The primary energy modulation caused by the optical pumping lasers was measured by using an electrostatic beam energy analyzer in the polarized source and an intensity profile monitor with 16 collector strips 2.5 mm wide, and with 3.0 mm spacing to measure beam position modulation downstream of the steering analyzing plates. The monitor was mounted on a remotely controlled swinging arm. Two measurements of coherent position modulation for the right and left monitor positions allowed separation of the energy and position modulation components of the OPPIS beam. An accuracy of 0.2 meV could be achieved in 10 min of integration time. The modulation magnitudes were quite sensitive to the pumping laser asymmetry between the two polarization states; after careful laser tuning, the coherent energy modulation was reduced to 1–2 meV and the coherent position modulation to the 20-nm level.

Although the frequent measurement of ΔE and dA_z/dE_{oppis} helped to set limits on the false A_z from energy modulation of the extracted proton beam, it is significant that the energy modulation of the extracted proton beam could not be measured directly at the parity apparatus. To cancel the effects of energy modulation, use was made of the fact that when the beam line helicity is reversed, the effects of true A_z reverse, but the effects of energy modulation do not. This is because energy modulation can only arise in the ion source and cyclotron. The magnets used to rotate the spin from up to positive helicity or up to negative helicity are downstream of all sources of energy modulation and do not affect the beam energy. Data were generally taken with alternating beam line helicity, and during the 1997 run data were also taken with the Wien filter reversed, an independent method of reversing the proton beam helicity relative to the ion source. The Wien filter and beam line settings are detailed in Table VII. That χ^2_ν for the 23 sets is only 1.08 following corrections, shows that the effects of uncorrected systematic errors, including energy modulation, were small. Care was taken to balance the amount of data taken in the two beam line helicities so that if some false A_z from energy modulation was present, it would tend to cancel in the final weighted average. Information on the energy modulation at the ion source and the sensitivity to this modulation was used to include the effects of uncorrected energy modulation in the error budget, as described in more detail in the following section.

VIII. METHOD OF APPLYING THE CORRECTIONS

The false A_z arising from a given coherent modulation was found by multiplying the measured modulation by the sensitivity to that modulation. Uncertainties from the variance of the corrected A_z distribution are referred to as ''statistical.'' The uncertainty quoted is the standard error in the mean of the A_z distribution. Uncertainties in A_z resulting from uncertainties in the sensitivities are referred to as ''systematic'' because an incorrect sensitivity will cause a systematic shift in the mean of the A_z distribution. These errors are, however, statistical in nature, as they arose from statistical uncertainties in the knowledge of the sensitivities to the various coherent modulations.

Table VIII summarizes the overall corrections to the parity data. To produce the 23 corrected A_z distributions shown in Fig. 6, the following procedure was followed.

(1) The data in each set were grouped into bundles of 10 000 event pairs per bundle.

(2) Each bundle was corrected according to the observed coherent modulations (except position and size) for that bundle, giving a corrected A_z for each bundle. The variance of corrected A_z values in a set determined an error bar for that set. This is reported as the statistical uncertainty. No corrections were made for position and size, because the net correction was consistent with zero and when the corrections were applied it was found that they slightly *increased* the residual correlations of A_z with position and size, as well as increasing the variance of the corrected A_z distribution.

(3) The uncertainties in the nil correction for position and size modulation were added in quadrature to each of the 23 sets. This is included in what is reported in Table VIII as systematic uncertainty.

(4) The uncertainties resulting from uncertainties in the various sensitivities were added in quadrature to the corresponding data. The uncertainties in the sensitivities are independent of what is accounted for in step (2), so it is justified to add them in quadrature to obtain the total error bar on each of the corrected A_z for the 23 sets. This uncertainty is also included in the systematic uncertainty in Table VIII.

(5) The A_z reported is the weighted mean of the 23 datasets with a weight $1/err^2$, where err is the ''total'' uncertainty, not including energy modulation. The error bars shown in the bottom panel of Fig. 6 are these total uncertainties.

(6) As mentioned earlier, the correction for extracted energy modulation was complicated by the fact that no direct measurement of energy modulation could be made in the parity beam line. The energy modulation sensitivities de-

TABLE VIII. Overall corrections for systematic errors. The table shows the average value of each coherent modulation, the net correction made for this modulation, and the uncertainty resulting from applying the correction.

Property	Average value	$10^7\Delta A_z$ (correction)
$A_z^{uncorrected}(10^{-7})$	1.68 ± 0.29(stat.)	
$y^*P_x(\mu\mathrm{m})$	-0.1 ± 0.0	-0.01 ± 0.01
$x^*P_y(\mu\mathrm{m})$	-0.1 ± 0.0	0.01 ± 0.03
$\langle yP_x\rangle(\mu\mathrm{m})$	1.1 ± 0.4	0.11 ± 0.01
$\langle xP_y\rangle(\mu\mathrm{m})$	-2.1 ± 0.4	0.54 ± 0.06
$\Delta I/I$(ppm)	15 ± 1	0.19 ± 0.02
Position + size		0 ± 0.10
ΔE (meV at OPPIS)	7–15	0.0 ± 0.12
Electronic crosstalk		0.0 ± 0.04
Total		0.84 ± 0.17(syst.)
$A_z^{corr}(10^{-7})$	0.84 ± 0.29(stat.)±0.17(syst.)	
$\chi^2_\nu(23\ sets)$	1.08	

pended on the beam line tune, so the distribution of measured OPPIS energy modulation values and dA_z/dE_{oppis} sensitivities was examined for a given beam line tune, and a correction and a ''worst case'' uncertainty in the correction were estimated.

Net corrections were calculated for energy modulation on a year by year basis. 1998 and 1999 required two corrections each, one for each beam line helicity. 1997 needed four corrections, as two Wien filter settings were used. Finally, all the energy modulation corrections were combined and one correction was applied to the final A_z.

The energy modulation correction shown in Table VIII is the net effect of energy modulation over the three runs. The net correction was zero. The ±0.12 uncertainty comes from the quadrature sum of the uncertainty in energy modulation plus the uncertainty in the energy modulation sensitivities. This was not included in the individual error bars for the 23 A_z numbers because the energy modulation was not known well enough. As a result, the reduced χ^2 of 1.08 for the 23 sets is larger than it really should be if the energy modulation uncertainty was determined individually for each of the 23 sets and included in the individual set by set error bars.

IX. RESULTS

The overall result for A_z from the 23 sets is summarized in Table VIII. After correcting for systematic errors, the longitudinal analyzing power is found to be $A_z=[0.84\pm0.29(\mathrm{stat.})\pm0.17(\mathrm{syst.})]\times10^{-7}$ at 221.3 MeV incident proton energy and the target and detector geometry of this experiment. Correcting for finite geometry and target thickness (see Sec. III C 2) and combining the errors in quadrature, gives $A_z=0.86\pm0.35$ at 225 MeV for comparison with theoretical calculations.

Parity violation in $\vec{p}p$ scattering has already attracted considerable theoretical interest, and many calculations of A_z have been made [28–32]. These calculations are shown in Fig. 13 together with the TRIUMF result (corrected to the $^1S_0$-$^3P_0$ zero crossing energy) and the most precise results at 13.6 MeV [5] and 45 MeV [4]. Theoretical predictions for A_z from several models are shown. The model of Driscoll and Miller [29] is based on the Bonn potential to represent the strong *N-N* interaction, together with the weak meson-nucleon coupling constants as given by Desplanques, Donoghue, and Holstein (DDH) [2]. The prediction of Iqbal and Niskanen [30] has a Δ isobar contribution added to the Driscoll and Miller model on a semi-*ad-hoc* basis. The theoretical prediction of Driscoll and Meissner [31] is based on a self-consistent calculation, with both weak and strong vertex functions obtained with a chiral soliton model. Finally, the quark model calculation of Grach and Shmatikov [32] takes explicit account of quark degrees of freedom. None of these predictions are in good agreement with the data, although they all have similar shapes due to the energy dependence of the strong interaction.

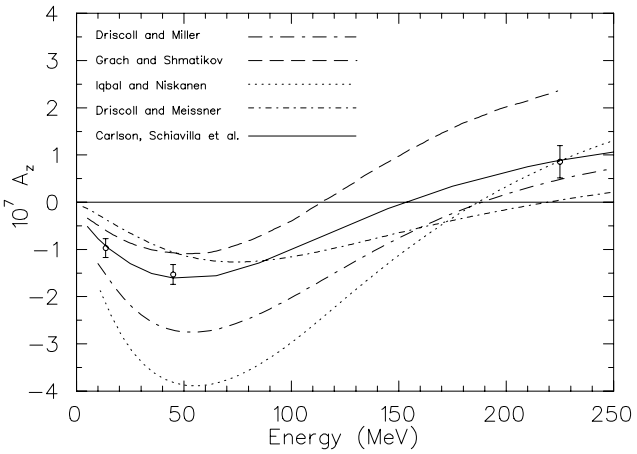

FIG. 13. Theoretical predictions for A_z and the most precise experimental data at 13.6 MeV (Bonn), 45 MeV (PSI), and 221 MeV (TRIUMF). The solid curve shows the results obtained by Carlson *et al.* by adjusting the weak coupling constants for the best fit to the experimental data.

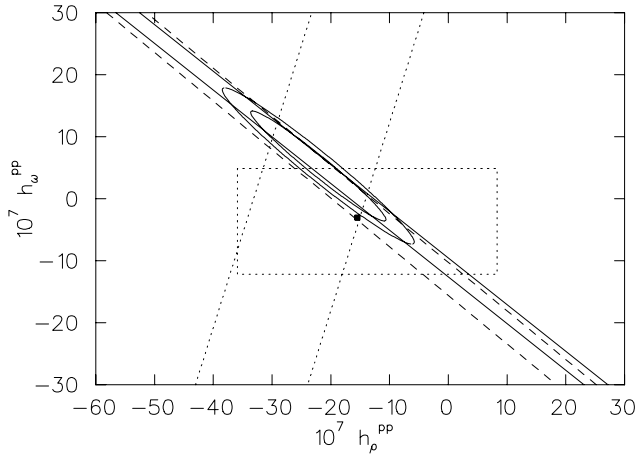

FIG. 14. Present constraints on the weak meson-nucleon couplings based on the experimental data and recent calculations by Carlson *et al.* [28]. The bands are the constraints imposed by different experiments (Bonn 13.6 MeV, dashed; PSI 45 MeV, solid; TRIUMF 221 MeV, dotted). The filled square and dotted rectangle are the DDH ''best guess'' and ''reasonable range,'' respectively. Also shown are the 68% and 90% C.L. contours.

A major source of uncertainty in these calculations is the value of the weak meson-nucleon couplings. Starting with the work of DDH [2], many theoretical calculations of these quantities were made [33–36] but theoretical uncertainties remained large. Until the TRIUMF experiment, the coupling constants were very poorly constrained by experiment.

Figure 14 shows the limits on the weak meson-nucleon couplings h_ρ^{pp} and h_ω^{pp} now imposed by the low-energy results [4,5] and the present TRIUMF result. The error bands are based on a calculation by Carlson *et al.* [28] assuming the Argonne v_{18} (AV-18) potential [37], the Bonn 2000 (CD-Bonn) [38] strong interaction coupling constants, and including all partial waves up to $J=8$. Although the TRIUMF measurement is not sensitive to A_z from SP mixing, and the contribution from PD mixing contains no h_ω^{pp} contribution, there is some h_ω^{pp} dependence arising from the higher partial wave mixings. The net result is that the acceptable band defined by the TRIUMF measurement is almost orthogonal to that defined by the low-energy measurements, and greatly reduces the acceptable ranges of both h_ρ^{pp} and h_ω^{pp}. Adjusting these coupling constants for the best fit to the pp data, including the TRIUMF 221-MeV point, Carlson *et al.* [28] estimate $h_\rho^{pp}=-22.3\times10^{-7}$ and $h_\omega^{pp}=5.17\times10^{-7}$, compared to the DDH ''best guess'' values of $h_\rho^{pp}=-15.5\times10^{-7}$ and $h_\omega^{pp}=-3.0\times10^{-7}$. The solid curve in Fig. 13 is calculated using the Carlson *et al.* adjusted couplings.

The reduction in the experimentally allowed range for weak meson-nucleon coupling constants also has implications for the analysis of electroweak radiative corrections in backward angle parity-violating electron scattering. By combining back angle electron scattering data for hydrogen [39] and deuterium [7], the SAMPLE Collaboration was able to extract values for both the isovector axial *e-N* form factor, $G_A^e(T=1)$, and the strange magnetic form factor, G_M^s at a momentum transfer $Q^2=0.1\ (\mathrm{GeV}/c)^2$. Their value $G_A^e(T=1)=+0.22\pm0.45\pm0.39$ differs significantly from the value $G_A^e(T=1)=-0.83\pm0.26$ arrived at by Zhu *et al.* [6] by applying one quark and many quark (proton anapole moment) radiative corrections to the well known nucleon axial charge as measured in neutron β decay. h_ρ^{pp} enters in the calculation of the proton anapole moment, but its contribution is small and one would require $h_\rho^{pp}\simeq-180\times10^{-7}$ to bring the value up to the $+0.22$ of the SAMPLE measurement. Such a value of h_ρ^{pp} is now clearly ruled out by the pp parity-violation data.

X. CONCLUSION

The parity-violating analyzing power A_z in $\vec{p}p$ elastic scattering has been measured at 221.3 MeV incident proton energy. The result constrains theoretical calculations of A_z in an energy region not previously covered experimentally. In the case of meson exchange calculations, it constrains principally the value of the weak ρ meson-nucleon coupling h_ρ^{pp}, but, when the low-energy $\vec{p}p$ data are included, strong constraints are placed on the acceptable values of both h_ρ^{pp} and h_ω^{pp}. This result has implications for the interpretation of other experiments. For example, it rules out incorrect values of these couplings as an explanation for the disagreement between the SAMPLE isovector axial form factor result [7] and the calculation of Zhu *et al.* [6].

ACKNOWLEDGMENTS

This work was supported in part by the Natural Sciences and Engineering Research Council of Canada, the U.S. Department of Energy, and the Russia-North America Scientific Collaboration Program; TRIUMF receives federal funding via a contribution agreement through the National Research Council of Canada.

[1] M. Simonius, Can. J. Phys. **66**, 548 (1988).
[2] B. Desplanques, J.F. Donoghue, and B.R. Holstein, Ann. Phys. (N.Y.) **124**, 449 (1980).
[3] M. Simonius, in *Interaction Studies in Nuclei*, edited by H. Jochim and B. Ziegler (North Holland, Amsterdam, 1975), p. 3; in *High Energy Physics with Polarized Beams and Targets*, edited by C. Joseph and J. Soffer (Birkhauser Verlag, Basel, 1981), p. 355.
[4] S. Kistryn *et al.*, Phys. Rev. Lett. **58**, 1616 (1987).
[5] P.D. Eversheim *et al.*, Phys. Lett. B **256**, 11 (1991); P. D. Eversheim (private communication).
[6] Shi-Lin Zhu, *et al.*, Phys. Rev. D **62**, 33008 (2000).
[7] R. Hasty *et al.*, Science **290**, 2117 (2000).
[8] D. Beck (spokesperson), Jefferson Lab Experiment Report No. 00-006.
[9] J. Birchall, S. A. Page, and W. T. H. van Oers (spokespersons), TRIUMF Experiment Proposal No. E497 1987.
[10] A. A. Hamian, Ph.D. thesis, University of Manitoba, 1998, see

http://www.triumf.ca/E497/archives/#Theses
[11] J. B. Bland, M.Sc. thesis, University of Manitoba, 2001, see http://www.triumf.ca/E497/archives/#Theses
[12] A.R. Berdoz *et al.*, Phys. Rev. Lett. **87**, 272301 (2001).
[13] W.T.H. van Oers, Int. J. Mod. Phys. **8**, 417 (1999).
[14] A. N. Zelenski *et al.*, in *Proceedings of the 12th International Symposium on High Energy Spin Physics*, edited by C. W. de Jager *et al.* (World Scientific, Amsterdam, 1997), p. 637.
[15] A.N. Zelenski *et al.*, in *Intersections Between Particle and Nuclear Physics*, edited by T. W. Donnelly, AIP Conf. Proc. **412** (AIP, Woodbury, NY, 1997), p.328.
[16] C. D. P. Levy *et al.*, in *Proceedings of the International Workshop on Polarized Beams and Polarized Gas Targets*, Cologne, 1995, edited by H. P. gen. Schieck and L. Sydow (World Scientific, Singapore, 1996), p. 120; A. N. Zelenski, *ibid.*, p. 111.
[17] S. D. Reitzner, M.Sc. thesis, University of Manitoba, 1996, see http://www.triumf.ca/E497/archives/#Theses
[18] A. N. Zelenski, *et al.*, *Proceedings of the 15th International Conference on Cyclotrons and Their Applications*, Caen, France, 1998, edited by E. Baron and M. Lieuvin (Institute of Physics, Bristol, UK, 1999) p. 642.
[19] M. K. Craddock, TRIUMF design note TRI-DN-84-8 1984; G. M. Stinson, TRIUMF design note TRI-DN-84-3, 1984.
[20] R. Abegg and R. Schubank, TRIUMF design note TRI-DN-84-8, 1984.
[21] L. G. Greeniaus and J. Soukup, TRIUMF Design note TRI-DNA-81-1, 1981.
[22] C.A. Davis *et al.*, Phys. Rev. C **53**, 2052 (1996).
[23] CNS Data Analysis Center, http://gwdac.phys.gwu.edu/
[24] A.R. Berdoz *et al.*, Nucl. Instrum. Methods Phys. Res. A **307**, 26 (1991).
[25] A. M. Sekulovich, M.Sc. thesis, University of Manitoba, 1990.
[26] A.R. Berdoz *et al.*, Nucl. Instrum. Methods Phys. Res. A **457**, 288 (2001).
[27] T. J. Stocki, M.Sc. thesis, University of Alberta, 1993, see http://www.triumf.ca/E497/archives/#Theses
[28] J. Carlson, R. Schiavilla, V.R. Brown, and B.F. Gibson, Phys. Rev. C **65**, 035502 (2002); R. Schiavilla (private communication).
[29] D.E. Driscoll and G.A. Miller, Phys. Rev. C **39**, 1951 (1989); **40**, 2159 (1989).
[30] M.J. Iqbal and J.A. Niskanen, Phys. Rev. C **49**, 355 (1994).
[31] D.E. Driscoll and Ulf-G. Meissner, Phys. Rev. C **41**, 1303 (1990).
[32] I. Grach and M. Shmatikov, Phys. Lett. B **316**, 467 (1993).
[33] V.M. Dubovik and S.V. Zenkin, Ann. Phys. (N.Y.) **172**, 100 (1986).
[34] N. Kaiser and U-G. Meissner, Nucl. Phys. **A499**, 699 (1989).
[35] U-G. Meissner and N. Kaiser, Nucl. Phys. **A510**, 759 (1990).
[36] U-G. Meissner and H. Wiegel, Phys. Lett. B **447**, 1 (1999).
[37] R.B. Wiringa *et al.*, Phys. Rev. C **51**, 38 (1995).
[38] R. Machleidt, Phys. Rev. C **63**, 024001 (2001).
[39] D.T. Spayde *et al.*, Phys. Rev. Lett. **84**, 1106 (2000).